Effective size of scattering centers in a two-dimensional electron gas

T. Deruelle,* K. Ensslin,† and P. M. Petroff
Materials Department, University of California, Santa Barbara, California 93106

A. L. Efros‡
Department of Physics, University of California, Riverside, California 92521

F. G. Pikus
A. F. Ioffe Institute, 194021 Leningrad, U.S.S.R.

(Received 12 August 1991; revised manuscript received 9 December 1991)

The screening behavior of a two-dimensional electron gas (2DEG) subjected to a periodic lattice of scattering centers or "antidots" is investigated. We have obtained an exact solution for the nonlinear screening problem of a 2DEG containing a single antidot and we have worked out a Monte Carlo simulation method to solve the case of a periodic antidot lattice. We also provide general theoretical predictions concerning the depletion phenomenon in this system. The shrinkage of the effective antidot size with increasing carrier density of decreasing periodicity of the lattice has been calculated and compared with experimental results.

I. INTRODUCTION

The transport of electrons in a periodic lattice of scattering centers has been the focus of recent experimental and theoretical investigations.[1–6] The scattering centers we consider hereafter are called "antidots" because they locally create a repulsive potential acting on the two-dimensional electron gas (2DEG). Interesting phenomena have been observed, such as the inhomogeneity of the electron density between the antidots,[1] and the magnetoresistance oscillations caused by the antidots.[2,3] The effective size of the antidots as they interact with the electrons is crucial in all these experiments. Here we present a calculation that evaluates the antidot potential as screened by the electrons. Antidots have been fabricated in several ways, e.g., using Ga-focused ion-beam implantation,[1] a field effect via a spatially modulated gate,[2] and etching.[3] In this paper we present experimental results on the Ga-focused ion-beam implantation[1] method and compare them with the theory. The main features should also be applicable to other experiments. Using the theory of nonlinear screening developed by one of us [7,8] a self-consistent charge distribution has been found to determine the antidot size as a function of carrier density N_s in the two-dimensional electron gas (2DEG) and eventually antidot lattice periodicity. In agreement with the experiments, the calculation predicts a shrinkage of the size of the antidots as a function of increasing carrier density N_s of the 2DEG, as well as for decreasing periodicity p of the antidot lattice. In addition, we study experimentally the carrier density N_s of the 2DEG as a function of the front gate voltage V_g. We observe that the slope of the N_s versus V_g function is independent of the periodicity p and that the threshold gate voltage $V_{\rm th}=V_g$ $(N_s=0)$ increases first for large values of $p\sim 300-500$ nm (p decreasing from 500 to 300 nm), and saturates for small values of $p<200$ nm. These findings are qualitatively explained by the calculation emphasizing again the effect of the physical size of the antidots.

The experimental system we consider here is described in detail in Ref. 1. A GaAs-$Al_xGa_{1-x}As$ heterostructure is implanted with a Ga^+ focused ion beam. The beam diameter can be measured accurately at high beam currents and is 80 nm. Transport through a square antidot lattice is possible at periodicities down to $p=110$ nm, which indicates that the diameter of the damaged area in the vicinity of the 2DEG cannot be larger than 110 nm, but indeed has to be smaller to permit electron transport. Therefore we conclude that the damaged area is of the size of the beam diameter, ≈ 80 nm. The implanted pattern is periodic in the 2DEG plane and forms the array of scattering centers. A pronounced negative magnetoresistance is observed for low magnetic fields $B<1$ T. The analysis as described in detail in Ref. 1, allows for a measurement of the antidot size. In Fig. 1 the depletion radii as a function of carrier density for a range of periodicities are compared with the theoretical results which will be developed further; the carrier density was changed via a front gate voltage. Two trends in the data are noticed: the size of the antidots shrinks for increasing N_s, as well as for decreasing p. To understand this behavior we considered the following model. Electrons from the 2DEG are trapped after implantation in the heavily damaged regions. In the experiment, this is indicated by the considerable decrease of N_s after implantation. This decrease depends on the number of antidots per unit area. From the results of large periodicities $p=500$ nm, we find that about 100 electrons are trapped per antidot, which corresponds to a trap density of $\Sigma\approx 10^{13}$ cm^{-2} in the damaged area.[9] The creation of these strongly repulsive zones leads to a depleted region in the vicinity of the implanted

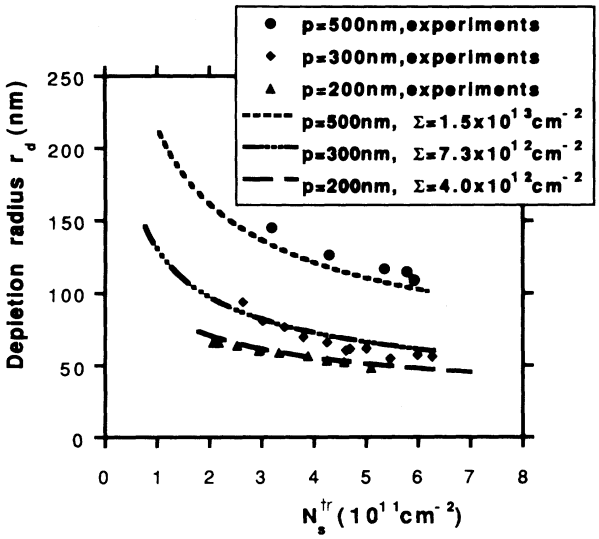

FIG. 1. Comparison of the experimental data showing the dependence of the depletion radius vs carrier density for different periodicities with the theoretical curves. The general behavior is the same as those which have been pointed out in Ref. 1. The plain curves correspond to the theoretical calculations. They represent the depletion radius as a function of the transport carrier density N_s^{tr}.

area: this is the lateral depletion layer. The carrier density N_s is deduced from the periodicity of the Shubnikov–de Haas oscillations at high magnetic fields and consequently represents the density of mobile carriers between the antidots. The estimation of Σ for samples with small values of p becomes more complicated, since the implanted area becomes comparable in size to the nonimplanted area.

By exciting carriers via the persistent photoconductivity effect we achieve, for a given photon dose, the same increase in N_s for the sample with antidots compared to the nonimplanted sample. This suggests that the amount of ionized Si dopants is unchanged by the implantation process. Our simplified model for these structures is as indicated in Fig. 2. Figure 2(a) presents the top view of the sample for large values of p where the depletion regions of the antidots do not touch each other. The central circle with radius a indicates the size of the implanted region, i.e., the beam size. The circle with radius r_d represents the limit of the depletion layer. The remaining area corresponds to the 2DEG. Figure 2(b) represents the cross-section view. The crosses indicate the positive charges N_+ of the Si donors, which are not affected by the implantation process and, therefore, are uniformly distributed. Inside the implanted columns the concentration of trapped electrons per area is denoted by Σ. Outside the depleted region, the electron density is nonzero but depends on the distance from the antidot. To make Fig. 2(b) clear, we have located the donor plane at its real position, 15 nm above the plane $z=0$ of the 2DEG. This distance is very small compared to the large antidot lattice periodicities (200 nm $< p <$ 500 nm) and the distance of the 2DEG from the surface (300 nm). Therefore, Fig. 2 reflects very well the situation for large antidot lattice

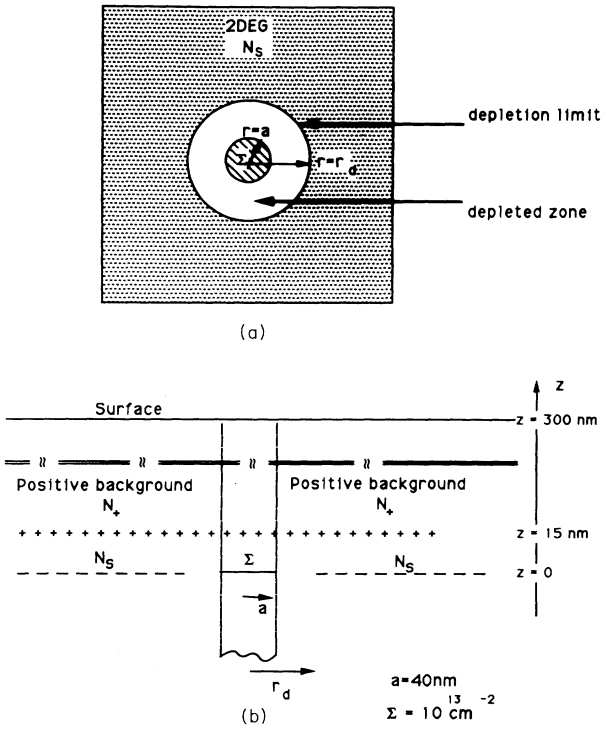

FIG. 2. Top and side views of the electrostatic system which approximates an antidot in a 2DEG structure.

periodicities and, in particular, for an infinite periodicity. We consider first a single antidot reflecting the situation of large periodicities.

The Fermi wavelength λ_F [for typical carrier densities $N_s=(2-4)\times10^{11}$ cm^{-2}, $\lambda_F=39-50$ nm] and the Thomas-Fermi screening length λ_0 ($\lambda_0=5$ nm) are much smaller than p. In this case we can use the theory of nonlinear screening.[7,8]

In Sec. II, we have obtained an analytical solution for the case of a single antidot. In Sec. III, we describe the results of a computer simulation applied to an antidot lattice. The comparison with the experimental data is discussed in Sec. IV.

II. ANALYTICAL SOLUTION FOR A SINGLE ANTIDOT

The approximation of a smooth external potential requires that the plane of the 2DEG be partitioned into two kinds of regions.[7,8]

(a) Metallic regions, where the electrostatic potential is constant and the electron density is nonzero (the theory of nonlinear screening assumes that the density of states of the 2DEG is infinite and therefore neglects the potential variations in the regions that are occupied by electrons).

(b) Dielectric regions where the electron density is zero (the large potential variations must occur in these regions and, moreover, the potential there must be repulsive).

In the case of a single antidot, the dielectric region (depleted zone) is the disk of radius r_d around the original implanted region (see Fig. 2). The depletion radius r_d and the electron density in the metallic region must be

the solution of the following nonlinear electrostatic problem. We must find the electrostatic potential $\Phi(r,z)$ that obeys the Laplace equation in the three-dimensional space and the following boundary conditions in the plane of the 2DEG ($z=0$):

$$(-e)\Phi(r,0)=\mu \tag{1}$$

at $r>r_d$, where μ is the chemical potential, and e the absolute value of the electron charge.

$$\left[-\frac{\partial\phi}{\partial z}\right]_{z=0+}-\left[-\frac{\partial\phi}{\partial z}\right]_{z=0-}=\frac{\sigma^{\text{ext}}(r)}{\varepsilon} \tag{2}$$

at $r<r_d$, where $\sigma^{\text{ext}}(r)$ is the external charge density at $r<r_d$ and ε the dielectric constant.

$$(-e)\Phi(r,0)>\mu \tag{3}$$

at $r<r_d$. In the case of a single antidot in a system of infinite extension, the electrostatic potential is chosen to vanish at an infinite distance from the antidot center. In this first section, $\mu=0$. We have kept it in the text to be consistent with Sec. II.

In the present case, $\sigma^{\text{ext}}(r)=-e(\Sigma-N_+)$ at $r<a$ with $\Sigma>N_+$, so that the electrons are repulsed from the disk of radius a and $\sigma^{\text{ext}}(r)=eN_+$ at $a<r<r_d$, where Σ is the trap density, N_+ the positive background density, r_d the depletion radius, and a the radius of the damaged area. For a single antidot, the electroneutrality condition implies that N_+ also represents the electron density at very large distance from the antidot.

It has been shown[7] that this problem has a unique solution. We have found it in the form[10]

$$\Phi(r,z)=\int_0^\infty dk\ A(k)J_0(kr)e^{-k|z|}-\frac{\mu}{e}\ , \tag{4}$$

where J_0 is the zeroth-order Bessel function of the first kind. We write $A(k)$ in the form

$$A(k)=\int_0^{r_d} f(t)\sin(kt)dt \tag{5}$$

so that condition (1) is satisfied:

$$\Phi(r,0)+\frac{\mu}{e}=\int_0^{r_d} f(t)dt\int_0^\infty J_0(kr)\sin(kt)dk=0\ , \tag{6}$$

since[11]

$$\int_0^\infty J_0(kr)\sin(kt)dk=0\quad\text{at } t<r\ . \tag{7}$$

Condition (2) leads to the integral equation which defines $f(t)$; indeed, after integrating $A(k)$ by parts in the form

$$k\,A(k)=f(0)-f(r_d)\cos(kr_d)+\int_0^{r_d}dt\frac{df}{dt}\cos(kt)\ ,$$

we obtain the total density of charge for all r:

$$\sigma^{\text{ext}}(r)=\frac{2\varepsilon f(0)}{r}+2\varepsilon\int_0^r\frac{dt}{\sqrt{r^2-t^2}}\frac{df}{dt}\quad\text{at } r<r_d\ , \tag{8}$$

$$\sigma(r)=\frac{2\varepsilon f(0)}{r}-\frac{2\varepsilon f(r_d)}{\sqrt{r^2-r_d^2}}+2\varepsilon\int_0^{r_d}\frac{dt}{\sqrt{r^2-t^2}}\frac{df}{dt}$$

$$\text{at } r>r_d\ . \tag{9}$$

Equation (8) leads to the complete determination of $f(t)$. After imposing $f(0)=0$ [$f(0)\neq 0$ would induce a divergence in the potential at $r=0$; see the Appendix], we get the solution

$$\frac{df}{dt}=\frac{1}{\pi\varepsilon}\frac{d}{dt}\int_0^t\frac{r\sigma^{\text{ext}}(r)}{\sqrt{t^2-r^2}}dr \tag{10}$$

and, therefore, with $f(0)=0$, one gets

$$f(t)=\frac{1}{\pi\varepsilon}\int_0^t\frac{r\sigma^{\text{ext}}(r)}{\sqrt{t^2-r^2}}dr\ . \tag{11}$$

We find $f(t)$ at $t<r_d$ at $t<a$

$$f(t)=-\frac{e(\Sigma-N_+)t}{\pi\varepsilon}\ , \tag{12}$$

at $a<t<r_d$

$$f(t)=\frac{e\Sigma\sqrt{t^2-a^2}-e(\Sigma-N_+)t}{\pi\varepsilon}\ . \tag{13}$$

The total charge density (electrons plus positive background) at $r>r_d$ is given by $\sigma(r)=\sigma^{\text{el}}(r)+eN_+$ [where $\sigma^{\text{el}}(r)$ is the electron density],

$$\sigma(r)=-\frac{2\varepsilon f(r_d)}{\sqrt{r^2-r_d^2}}+\frac{2}{\pi}e\Sigma\sin^{-1}\left[\left(\frac{r_d^2-a^2}{r^2-a^2}\right)^{1/2}\right]$$

$$-\frac{2}{\pi}e(\Sigma-N_+)\sin^{-1}\left[\frac{r_d}{r}\right]\ , \tag{14}$$

taking into account that

$$f(r_d)=\frac{e\Sigma\sqrt{r_d^2-a^2}-e(\Sigma-N_+)r_d}{\pi\varepsilon}\ ; \tag{15}$$

then the asymptotic behavior of $\sigma(r)$ at $r\gg r_d$ takes the form

$$\sigma(r)\approx\frac{2e\Sigma a^2\sqrt{r_d^2-a^2}}{3\pi r^3}\left[1-\frac{\pi\varepsilon f(r_d)r_d^2}{\Sigma a^2\sqrt{r_d^2-a^2}}\right] \tag{16}$$

(at $r\gg r_d$). On the other hand, when $r\to r_d$, $\sigma(r)\approx-[2\varepsilon f(r_d)/\sqrt{r^2-r_d^2}]$; if $f(r_d)<0$, then $\sigma(r)$ goes to $+\infty$ when $r\to r_d$; however, no other positive charges but the positive background are present in the system; therefore, the possible singularity at $r=r_d$ must come from the electron distribution. That means $f(r_d)\geq 0$.

Condition (3) leads to the determination of the unique value of r_d. Indeed, at $r<r_d$, the electrostatic potential is given by

$$\Phi(r,0)+\frac{\mu}{e}=\int_0^{r_d} f(t)dt\int_0^\infty J_0(kr)\sin(kt)dk$$

$$=\int_r^{r_d}\frac{dt}{\sqrt{t^2-r^2}}f(t) \tag{17}$$

so, according to condition (3), this must be negative at $r < r_d$.

Suppose $f(r_d) > 0$. Then, in the vicinity of r_d, at $r < r_d$,

$$\Phi(r,0)+\mu/e \approx f(r_d)\operatorname{arccosh}\left[\frac{r_d}{r}\right] .$$

This vanishes when $r \to r_d$, but remains positive at $r < r_d$, with $f(r_d) > 0$. This shows that the potential energy is smaller than the chemical potential μ in the vicinity of r_d, which clearly contradicts the third condition. Thus $f(r_d)=0$ is the equation that determines r_d. It is easy to check that, if such a condition is implemented, then $f(t)<0$ at $t < r_d$ and thus condition (3) is satisfied. Therefore, the correct expression for d is

$$r_d = a\left[\frac{\Sigma}{N_+}\right]^{1/2}\frac{1}{(2-N_+/\Sigma)^{1/2}} = a\left[\frac{\Sigma}{N_s}\right]^{1/2}\frac{1}{(2-N_s/\Sigma)^{1/2}} , \tag{18}$$

since $N_s = N_+$ in the case of a single antidot.

The total charge Q in the nondepleted region is derived from the following expression:

$$Q = \int_{r_d}^{\infty}\sigma(r)2\pi r\,dr = 2\pi\int_{r_d}^{\infty} r\left\{\frac{2}{\pi}e\Sigma\sin^{-1}\left[\left[\frac{r_d^2-a^2}{r^2-a^2}\right]^{1/2}\right] - \frac{2}{\pi}e(\Sigma-N_+)\sin^{-1}\left[\frac{r_d}{r}\right]\right\}dr \tag{19}$$

is equal to $e\Sigma\pi a^2 - eN_+\pi r_d^2$, which demonstrates the electroneutrality of this problem.

At very large r, the electronic density $\sigma^{el}(r)$ is not perturbed:

$$\sigma^{el}(r) = -eN_s = -eN_+ .$$

For the nonimplanted sample with $\Sigma = N_s = N_+$ this leads to $r_d = a$, i.e., no depletion length as it should be. In the implanted sample we have $\Sigma \gg N_+$ and, therefore,

$$r_d = \frac{a}{\sqrt{2}}(\Sigma/N_+)^{1/2} .$$

At this point, we would like to explain that important result. If we assume that the electron density is uniform in the nondepleted region and equal to $-N_+$, then the electroneutrality equation provides $r_d = a(\Sigma/N_+)^{1/2}$. The factor $\sqrt{2}$ originates from the nonuniformity of the electron density in the nondepleted region. Figure 3 shows the electron density vs the radial coordinate r provided by Eq. (13). At $r = a(\Sigma/N_+)^{1/2}$, the electron density is 70% of its asymptotic value, whereas the error in d is about 40% if we assume $r_d = a(\Sigma/N_+)^{1/2}$ instead of

$$r_d = \frac{a}{\sqrt{2}}(\Sigma/N_+)^{1/2} .$$

Another interesting result is the dependence of the potential barrier on the electron density. Formula (6) gives a means of calculating the electrostatic potential at $r < r_d$. Its expression is given in the Appendix. It follows that the drop of the electrostatic potential between the implanted cylinder and the nondepleted region is simply

$$\Delta E_0 = \frac{e^2\Sigma a^2}{\pi\varepsilon}\left[1-\frac{a}{r_d(N_+)}\right] . \tag{20}$$

This clearly shows that the more the electron density increases, the more the potential created by the ionized traps is screened.

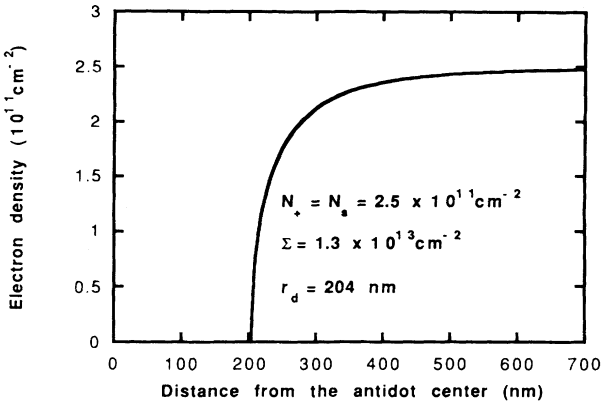

FIG. 3. Electron-density variation for a single antidot as a function of the distance from the antidot center. This plot is obtained for $\Sigma = 10^{13}$ cm^{-2} and $N_+ = 2.5\times10^{11}$ cm^{-2}.

For a rough comparison between experiment and theory, we choose $p = 512$ nm and $N_s = 2.5\times10^{11}$ cm^{-2}. The experiment reveals $r_d = 140$ nm (see Fig. 1 and Ref. 1). The theory for an infinite periodicity with $\Sigma = 10^{13}$ cm^{-2}—which has been evaluated experimentally—gives $r_d = 180$ nm in reasonable agreement with the experiment. Also, the theory predicts a decrease of the depletion radius with increasing N_s as observed in the experiment.

III. NUMERICAL SOLUTION FOR AN ANTIDOT LATTICE

To study the periodicity effect of this system, we have worked out a program and adapted it to a periodic lattice of repulsive centers, or antidots. The theoretical basis for this numerical solution has been explained previously in the study of a single antidot. It solves this problem on a unit cell, i.e., a square grid of length p, of $N\times N$ sites, assuming periodic-boundary conditions:[12,13] the initial square is periodically repeated along each coordinate axis so that all the calculated functions in this program (in particular the electron density and the electrostatic potential) are invariant under any translation of length p; thus we have checked that the solution of the problem involving four antidots in a square cell of length $2p$ is the same as the one involving one antidot in a square cell of length p. Figure 4 outlines the procedure. The computation starts with the case of a single disk of radius a and

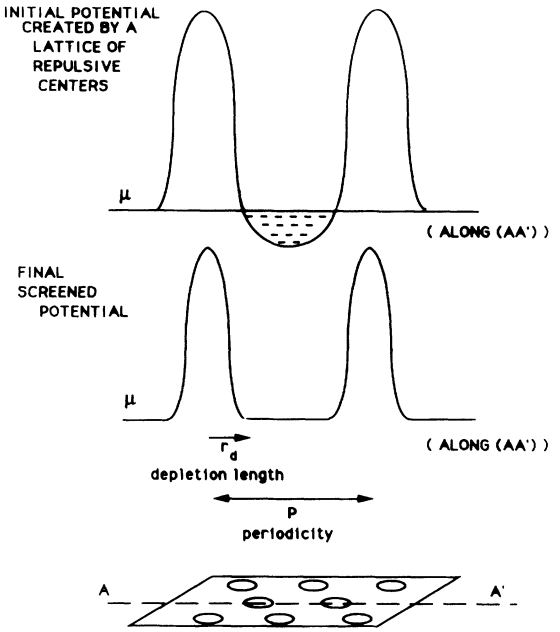

FIG. 4. Basis of the numerical solution.

density Σ, in the center of a square, with the positive background associated with the initial charge. We impose a given value of the chemical potential μ at the very beginning and the program finds the density of electrons that obeys the conditions required by the theory. In such a way, we simulate the change of potential of the gate electrode when the distance between the surface and the 2DEG is much larger than the depletion region size. The potential valleys defined by this value of μ are progressively filled with electrons until their potential energy reaches that value. For every iteration, we impose the charge neutrality onto the system. In other words, when a number δn of electrons is added to the system, the amount δn is *uniformly* redistributed to the positive background all over the unit square. The iteration stops when the electrostatic energy of the 2DEG reaches the imposed value μ. Therefore, for each value of μ we get a unique corresponding carrier density N_s and a unique depletion zone.

The computation first indicates the existence of different regimes in this system, for all periodicities p and all trap densities Σ (see Fig. 5).

(1) A regime where the unit cell is partially filled with electrons. In this regime, the electrons are located in pockets around the corners. At zero temperature, the system is therefore a complete insulator in this regime [see Fig. 5(a)].

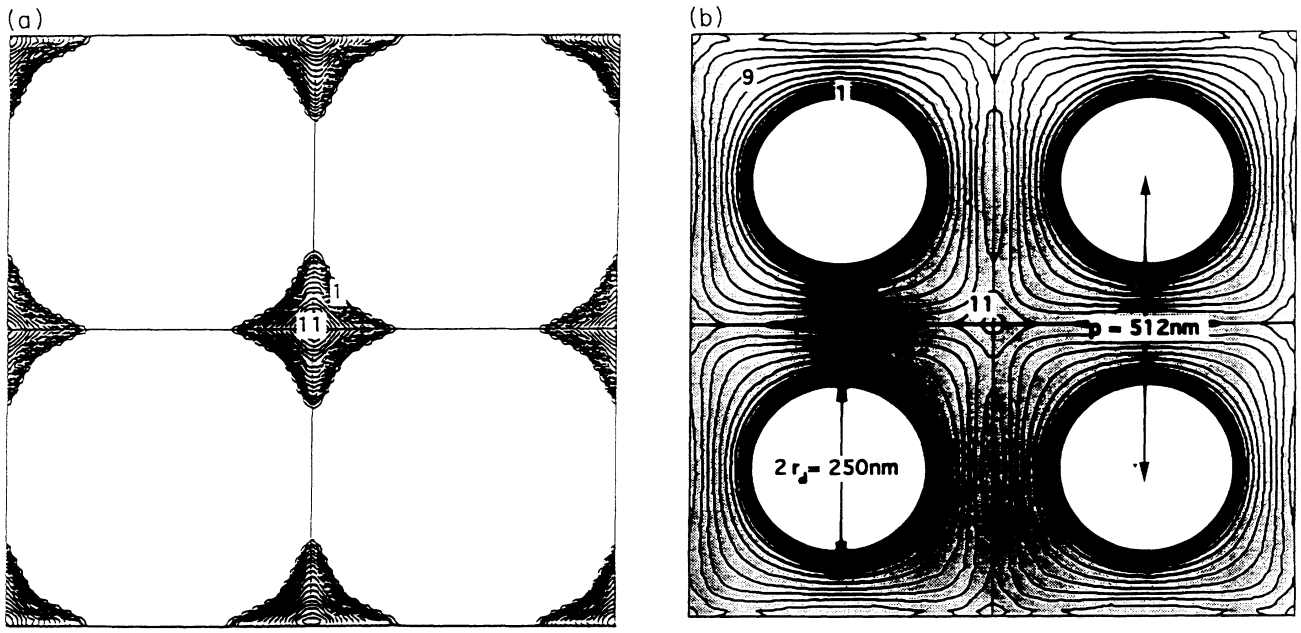

FIG. 5. The following plots represent the electron density plotted vs the spatial coordinates and obtained by the computer simulation. Shaded areas in (b) indicate electron-filled regions. (a) shows some isoelectron-density lines in the insulating regime where the existence of electron pockets is revealed. Only the first neighbors are represented in this picture. In this case, the average electron density is 0.3×10^{11} cm^{-2}. Isodensity line 1 represents the line at which the electron density vanishes. On isoelectron density line 11, the electron density almost reaches its maximum, here 0.5×10^{11} cm^{-2}. (b) Above a certain critical electron density, the conduction regime is reached. The conduction channels start growing. With increasing carrier densities,the width of the channel in between two antidots increases or, in other words, the depletion radius shrinks. Isoelectron density line 1 is the depletion limit at $d=125$ nm. The electron density then increases until it reaches its limit value on the borders of the cell. On isoelectron density line 11, the electron density is close to its maximum value: 4×10^{11} cm^{-2}. At isoelectron density line 9, the electron density takes approximately the value of the average electron density.

(2) Above a certain critical average electron density N_s^c, there is a regime where a disk of radius r_d (the depletion length) is depleted of electrons and where the existence of a channel allows the transport of electrons. This is the conduction regime [see Fig. 5(b)].

In the insulator regime, the depletion diameter $2r_d$ is larger than the periodicity p, and the electron density between two antidots is zero. Therefore, at zero temperature, no transport is allowed and the system is an insulator. In the conduction regime, the electron density can either be measured from the Shubnikov–de Haas oscillations or from the Hall effect. However, the electron density in this system is inhomogeneous. For a given magnetic field, the filling factor of the Landau levels is also spatially dependent. The region of the maximum filling factor is centered at the corners of the unit cells since the electron density is always maximum at this point (see Fig. 5). The boundaries of this region (edge trajectories) can be either closed or opened.[14] The corresponding Landau level contributes to the transport only if they are open. This occurs when that level starts being filled with electrons at the saddle point which is the point in between two neighboring antidots. Thus, the most important density for the transport is the density in between two neighboring antidots, since it is the passing point for the current. We refer to the density at this point as the "transport" density N_s^{tr}. This density is responsible for the period of the oscillations of the transport coefficients. It equals zero when the average electron density is N_s^c and the positive background density reaches its threshold value, N_+^{th}; this is the transition from the insulator regime to the conductor regime. For Landau levels of larger indices, one can expect that the quantization is not very important for the screening properties. Otherwise, it must be taken into account.

Strictly speaking, N_s^{tr} should not be linear with the gate voltage, and the oscillations should not be periodic with the gate voltage, either. However, we show in Sec. IV that in our experiments, the linearity exists. We discuss

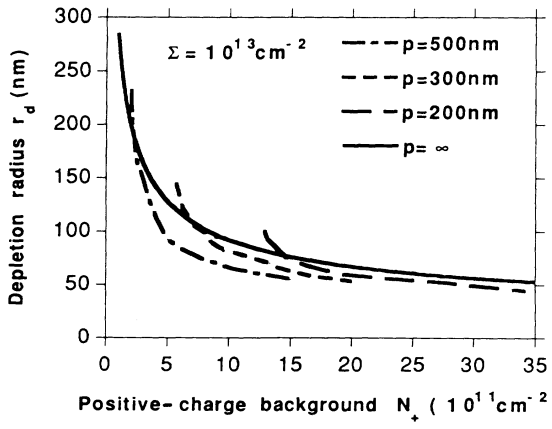

FIG. 6. Depletion radius vs applied positive background: numerical solution; the depletion radius shrinks with increasing N_+ (and, therefore, with increasing average electron density). The analytical solution is valid in a large range of densities.

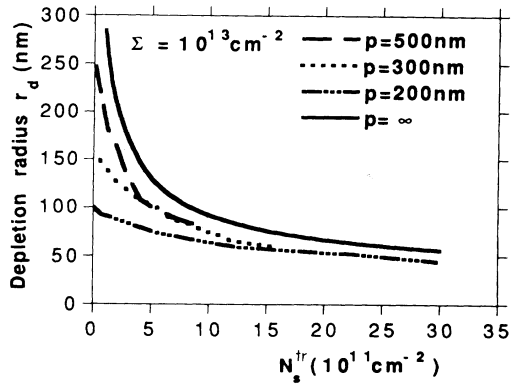

FIG. 7. Depletion radius vs the transport density: numerical solution; the behavior is the same as that of Fig. 6, since increasing the positive charge background implies increasing the electron density and therefore reducing the depletion radius.

hereafter the variations of different parameters in this system at a constant trap density $\Sigma = 10^{13}$ cm^{-2}.

In Fig. 6, the variations of the depletion radius vs the positive background N_+ are represented for three periodicities p. It shows that the depletion radius shrinks with increasing N_+ (therefore, with increasing carrier densities) and that it does not depend on the antidot lattice periodicity for large values of N_+. Moreover, the analytical expression obtained for an infinite periodicity, which has to be the asymptotic value, is valid in a large range. A dependence on the periodicity is observed at low N_+, since the maximum value of the depletion radius in the conduction regime is half the periodicity.

Figure 7 compares the variations of the depletion radius vs the transport density. At very large carrier densities the system tends to be uniform while the depletion radius shrinks; it is clear that, in both cases (Figs. 6 and 7) the asymptotic behavior of the depletion radius must

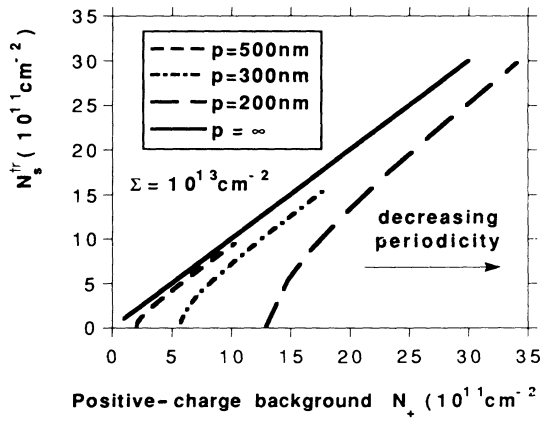

FIG. 8. Transport density N_s^{tr} as a function of positive background density: numerical solution; we observe an increasing shift of the threshold background density (at $N_s^{tr}=0$) with decreasing periodicities. The simulation has been achieved for $\Sigma = 1\times10^{13}$ cm^{-2}. For intermediate N_+, the regime is quasilinear before all the curves take an identical asymptotic behavior.

not depend on the periodicity.

Finally, we present in Fig. 8 the variations of the transport density vs the positive background. At large positive background densities, we observe a similar behavior for the studied periodicities. In this range of densities, the depletion radius tends to the value of the beam diameter, $a=40$ nm and, therefore, the system behaves like a regular condensor.

The shift in the threshold positive background density $N_+^{\rm th}$ at $N_s^{\rm tr}=0$ varies approximately as $1/p^2$. In the following section, this type of dependence will be explained in more detail.

IV. COMPARISON WITH EXPERIMENTAL RESULTS

Figure 9 shows the dependence of the carrier density, measured from the periodicity of the Shubnikov–de Haas oscillations, vs the applied gate voltage for different periodicities p of the antidot lattice. Three striking observations need to be explained: (a) the apparent parallelism of those curves in this range of carrier densities; (b) the shift of the threshold gate voltage $[V_g(N_s=0)]$ with decreasing periodicities; (c) the saturation of the threshold voltage at periodicities smaller than $p=200$ nm.

Behaviors (a) and (b) are predicted in Sec. III (see Fig. 8). Indeed, we have underlined the increasing shift of the threshold positive background with decreasing periodicities. This shift varies approximately as $1/p^2$ and should saturate when the antidot lattice periodicity gets closer to the beam diameter (80 nm). However, in Fig. 9, the saturation occurs when the periodicity decreases from $p=200$ nm. This clearly shows that the ionized trap density does depend on the periodicity, at least for small periodicities. But, as mentioned earlier, it is more difficult to estimate Σ for smaller periodicities because the implanted area becomes the size of the nonimplanted area. In fact, the charge-neutrality equation shows that $\Sigma(p)$ has to be proportional to p^2 in order to account for the observed saturation at $p<200$ nm.

A simple explanation of this parabolic dependence is given in the following. When the antidot lattice periodicity is reduced in a given large area, the number of created defects increases. Therefore, if we assume that the average number of electrons trapped after implantation is the same in this large area for $p<200$ nm, then the average ionized trap density per unit cell must decrease with the periodicity and is given by $\Sigma(p)=\Sigma(200\ \text{nm})(p/200)^2$ (with p in nm).

On the other hand, at very large antidot lattice periodicities, the charged trap density must tend to its asymptotic value when p is infinite. To determine the intermediate experimental values of $\Sigma(p)$ at $p=500$ nm, $p=300$ nm, and $p=200$ nm, we have adjusted them from Figs. 8 and 9 in the following way. Suppose that the ionized donor density is p independent, as said earlier; we are able to determine $\Sigma(p)$ from the experimental data. Indeed, at a given gate voltage for different periodicities p, the difference of measured carrier densities $\Delta N_s^{\rm tr}$ can be related to the variation of ionized trap densities $\Delta[\Sigma(p)/p^2]$ by the following relation derived from the charge-neutrality equation:

$$\Delta N_s^{\rm tr}=-\pi a^2\Delta\left[\frac{\Sigma(p)}{p^2}\right], \tag{21}$$

which is valid at large positive background densities, when $N_s^{\rm tr}$ is close to the average electron density. This clearly proves that Σ decreases with p according to Fig. 9.

Finally, if we know, for example, $\Sigma(500\ \text{nm})$, we can afterwards deduce $\Sigma(300\ \text{nm})$ and $\Sigma(200\ \text{nm})$ using Fig. 9 and Eq. (21) (at large electron densities). At $p>500$ nm, $\Sigma(p)$ must saturate to its value for an infinite periodicity. To determine $\Sigma(500\ \text{nm})$, we fit the experimental curve of Fig. 1 and we find $\Sigma(500\ \text{nm})=1.5\times10^{13}\ \text{cm}^{-2}$.

Summarized in Fig. 10 is the dependence of Σ on the

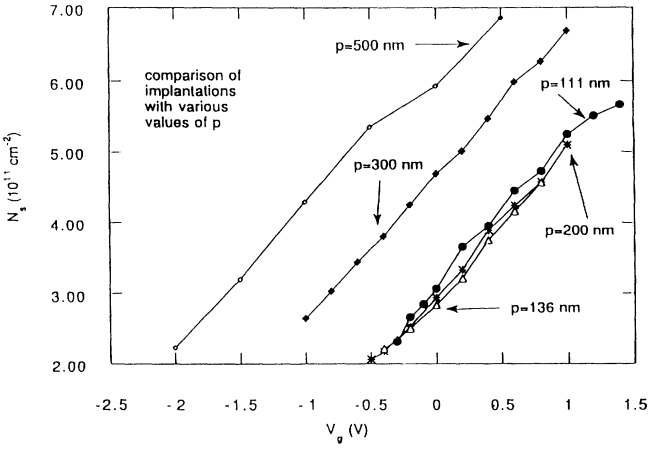

FIG. 9. Experimental data showing the carrier density measured with the periodicity of the Shubnikov–de Haas oscillations as a function of the applied gate voltage. The parallelism of those curves, the shift of the threshold gate voltage at low carrier densities increasing with decreasing periodicities, and the saturation at periodicities <200 nm are noted.

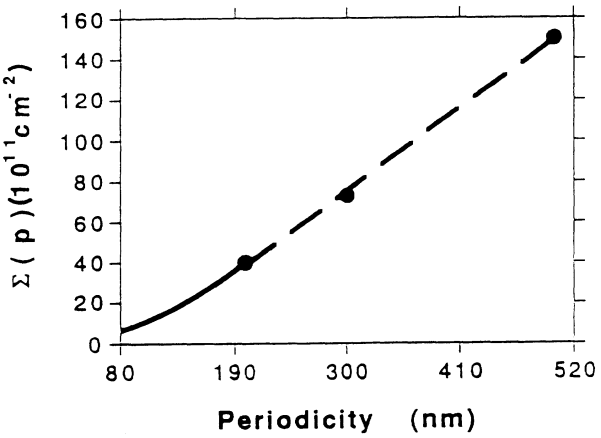

FIG. 10. Periodicity dependence of the ionized trap density which has been deduced from Figs. 8 and 9. We note the parabolic behavior (plain curve) for $p<200$ nm, which accounts for the observed saturation. For $p>500$ nm, the trap density should progressively saturate to the value Σ ($p=\infty$).

periodicity p. We do not know quantitatively the ionized-donor concentration; therefore, we can only show in Fig. 11 the dependence of the transport density on the positive background, which is provided by the numerical calculation. It reproduces the periodicity dependence shift in the threshold positive background when N_s^{tr} decreases, with (a) a $1/p^2$-type dependence at large periodicities since the trap density does not depend strongly on p, and (b) a saturation in the shift at $p < 200$ nm. Finally, Fig. 11 points out the linear behavior of N_s^{tr} vs N_+ in the range of applied positive background densities 2×10^{11} cm^{-2}–7×10^{11} cm^{-2}, the slope of those curves being slightly dependent on the periodicity.

Finally, we have checked that the deduced values of $\Sigma(p)$ for $p = 300$ and 200 nm from Fig. 9 could enable us to reproduce the experimental data of Fig. 1 showing the depletion radius as a function of the transport density. Actually, the depletion effect can be directly pointed out from transport experiments,[1] and it has been shown that features in the longitudinal magnetoresistance as a function of the magnetic field could lead to its evaluation (see Ref. 1 for its experimental determination). In Fig. 1, the theoretical dependence of the depletion radius on the transport density in the channel is compared to the experimental measurements for the periodicities 500, 300, and 200 nm. The values of $\Sigma(p)$ are indicated in the legend frame. We notice again that an increase of the gate voltage enhances the average carrier density (and, therefore, the transport density) and reduces the effective antidot size. Finally, the good agreement between experiment and theory reinforces the idea that, in this very inhomogeneous system, transport properties are determined by the geometrical place where the current is the most strongly subjected to the antidot repulsion.

In conclusion, we have shown that the electron density in an antidot lattice is quite inhomogeneous in certain cases,[1] at least in the vicinity of the depleted zone. In this regard, we do not expect the electron gas to behave like a free 2DEG. In particular, we think that the electron concentration in between two antidots has a crucial role in the transport properties of this system. However, at large carrier densities, when the depleted zone is expected to be considerably reduced by the screening effect, we think that the transport properties must resemble those of an homogeneous 2DEG.

We have compared experimentally determined values of the antidot size with the results of a self-consistent electrostatic calculation. The agreement is satisfactory. We have pointed out that this effective size can be adjusted via an applied gate voltage (or using photons, as in Ref. 1) that modifies the positive background and, therefore, the average electron density. At small periodicities, the physical size of the antidot is not determined mainly by depletion effects but by the present states of the fabrication technology, i.e., the focused-ion-beam diameter.

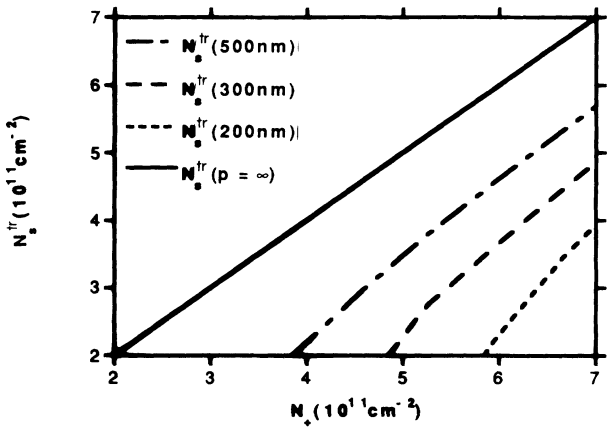

FIG. 11. Variation of the transport density vs the positive background density provided by the numerical calculation. Knowing the ionized donor density, we could fit Fig. 9 (assuming an unchanged capacitance).

ACKNOWLEDGMENTS

We thank Professor L. J. Sham for valuable discussions and acknowledge financial support from Thomson-CSF, the U.S. Air Force, and QUEST, an NSF science and technology center.

APPENDIX

At $r < r_d$, the electrostatic potential is given by

$$\Phi(r,0)+\frac{\mu}{e}=\int_0^{r_d} f(t)dt \int_0^{\infty} J_0(kr)\sin(kt)dk$$
$$=\int_r^{r_d}\frac{f(t)}{\sqrt{t^2-r^2}}dt$$

(see Ref. 11). In particular,

$$\Phi(0,0)+\frac{\mu}{e}=\int_0^{r_d}\frac{f(t)}{t}dt$$

which shows that $f(0)$ must be equal to zero for the potential at $r=0$ to be finite. Thus, at $r < a$

$$\Phi(r,0)+\frac{\mu}{e}=\frac{e\Sigma a}{\pi\varepsilon}\left[E\left[\sin^{-1}\left[\frac{a}{r_d}\right],\frac{r}{a}\right]-E\left[\frac{r}{a}\right]\right],$$

at $a < r < r_d$,

$$\Phi(r,0)+\frac{\mu}{e}=\frac{e\Sigma r}{\pi\varepsilon}\left\{\left[1-\frac{a^2}{r^2}\right]\left[K\left[\frac{a}{r}\right]-F\left[\sin^{-1}\left[\frac{r}{r_d}\right],\frac{a}{r}\right]\right]+E\left[\sin^{-1}\left[\frac{r}{r_d}\right],\frac{a}{r}\right]-E\left[\frac{r}{a}\right]\right\},$$

where $E(x,y)$ is the elliptic integral of the second kind, $E(x)$ is the complete elliptic integral of the second kind, $F(x,y)$ is the elliptic integral of the first kind, and $K(x)$ is the complete elliptic integral of the first kind.

*Permanent address: Ecole Normale Supérieure, 24 rue Lhomond, 75005 Paris, France.
†Permanent address: Sektion Physik der Universitaet München, Geschwister-Scholl-Platz 1, 8000 München 22, Bundes Republik Deutschland.
‡Permanent address: Department of Physics, University of Utah, Salt Lake City, UT 84112.

[1]K. Ensslin and P. M. Petroff, Phys. Rev. B **41**, 12 307 (1990).
[2]H. Fang and P. J. Stiles, Phys. Rev. B **41**, 10 171 (1989).
[3]R. W. Winkler and J. P. Kotthaus, Phys. Rev. Lett. **62**, 1177 (1989).
[4]K. Kern, D. Heitmann, P. Granbow, Y. H. Zhang, and K. Plogg, Phys. Rev. Lett. **66**, 1618 (1991).
[5]R. R. Gerhardts, D. Weiss, and K. v. Klitzing, Phys. Rev. Lett. **62**, 1173 (1989).
[6]D. Weiss, M. L. Roukes, A. Menschig, P. Grambow, K. v. Klitzing, and G. Weimann, Phys. Rev. Lett. **66**, 2790 (1991).
[7]A. L. Efros, Solid State Commun. **67**, 11, 1019 (1988).
[8]A. L. Efros, Solid State Commun. **70**, 03, 253 (1989).
[9]Actually, those repulsive traps are distributed in volume and their distribution must have a pronounced peak around the donor plane. But since the radius of the cylinder and the distance between the plane of donors and the plane of the 2DEG are negligible compared to the large antidot lattice periodicities ($p \approx 300-500$ nm), we suppose that those traps are distributed on a disc of diameter 80 nm, of charge Σ per cm^{-2}.
[10]K. N. Sneddon, *Mixed Boundary Value Problems in Potential Theory* (North-Holland, Amsterdam, 1966).
[11]I. S. Gradshteyn and I. M. Ryzhik, *Table of Integrals, Series, and Products* (corrected and enlarged edition) (Academic, New York, 1980), p. 731.
[12]E. I. Levin, V. I. Nguen, B. I. Shklovsii, and A. L. Efros, Zh. Eksp. Teor. Fiz. **92**, 1499 (1987) [Sov. Phys. JETP **65**, 842 (1987)].
[13]J. H. Davies, P. A. Lee, and T. M. Rice, Phys. Rev. Lett. **49**, 758 (1982).
[14]M. Buttiker, Phys. Rev. B **38**, 9375 (1988).

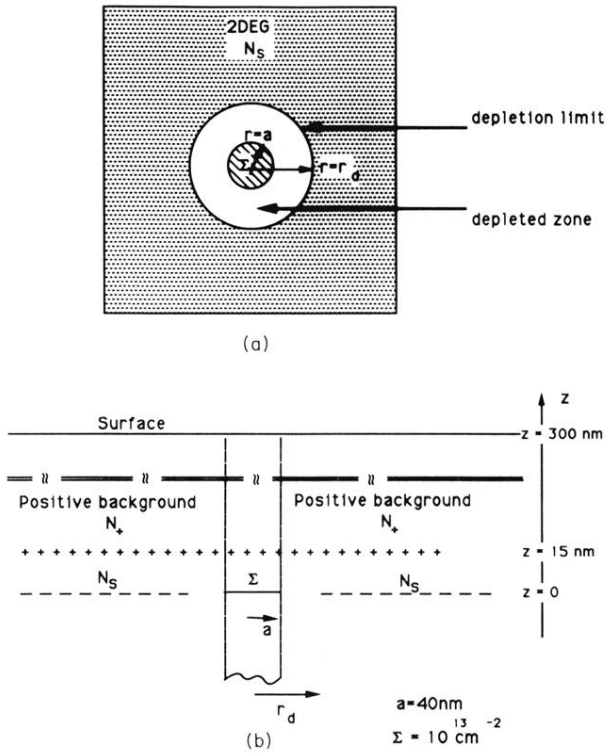

FIG. 2. Top and side views of the electrostatic system which approximates an antidot in a 2DEG structure.

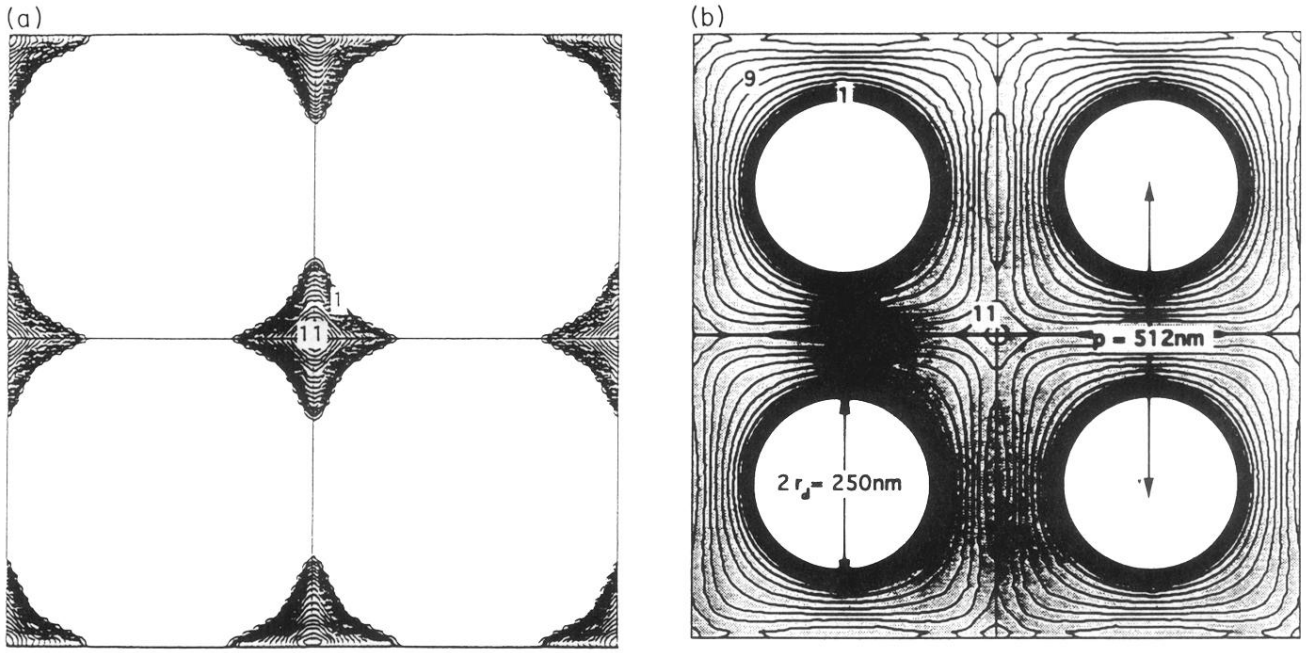

FIG. 5. The following plots represent the electron density plotted vs the spatial coordinates and obtained by the computer simulation. Shaded areas in (b) indicate electron-filled regions. (a) shows some isoelectron-density lines in the insulating regime where the existence of electron pockets is revealed. Only the first neighbors are represented in this picture. In this case, the average electron density is 0.3×10^{11} cm^{-2}. Isodensity line 1 represents the line at which the electron density vanishes. On isoelectron density line 11, the electron density almost reaches its maximum, here 0.5×10^{11} cm^{-2}. (b) Above a certain critical electron density, the conduction regime is reached. The conduction channels start growing. With increasing carrier densities,the width of the channel in between two antidots increases or, in other words, the depletion radius shrinks. Isoelectron density line 1 is the depletion limit at $d=125$ nm. The electron density then increases until it reaches its limit value on the borders of the cell. On isoelectron density line 11, the electron density is close to its maximum value: 4×10^{11} cm^{-2}. At isoelectron density line 9, the electron density takes approximately the value of the average electron density.